

Do we need up/down decomposition for Marchenko imaging?

Kees Wapenaar*, Delft University of Technology; Roel Snieder, Colorado School of Mines; Sjoerd de Ridder, University of Leeds; Evert Slob, Delft University of Technology

Summary

Marchenko redatuming, imaging, monitoring and multiple elimination methods are based on Green's function representations, with the underlying assumption that the wave field in the subsurface can be decomposed into downgoing and upgoing waves and that evanescent waves can be neglected. In this paper we show that up/down decomposition in the subsurface is actually not needed for the derivation of these representations. This opens the way for research into new Marchenko methods which are not limited by the assumption that up/down decomposition is possible and which, in principle, can handle evanescent waves.

Introduction

Current Marchenko methods for seismic redatuming, imaging, monitoring and multiple elimination (Ravasi et al., 2016; Staring et al., 2018; Jia et al., 2018; Lomas and Curtis, 2019; Mildner et al., 2019; Brackenhoff et al., 2019; Zhang and Slob, 2020; Elison et al., 2020; Reinicke et al., 2020) are derived from representation integrals for up/down decomposed wave fields (Slob et al., 2014; Wapenaar et al., 2014). Promising applications in large-scale problems have been developed (Pereira et al., 2019; Staring and Wapenaar, 2020; Ravasi and Vasconcelos, 2020). Of course there are also limitations, some of them caused by the underlying assumption that the wave fields inside the medium can be decomposed into downgoing and upgoing waves and that evanescent waves inside the medium can be neglected.

Recently, several approaches have been proposed to circumvent up/down decomposition inside the medium in the derivation of Marchenko methods (Kiraz et al., 2020; Diekman and Vasconcelos, 2021; Wapenaar et al., 2021), each with their own pros and cons. Here we discuss the last mentioned approach, which derives Green's function representations for the Marchenko method without up/down decomposition inside the medium, and we illustrate these representations with numerical examples. A discussion of the application of these representations in new Marchenko methods is beyond the scope of this paper.

Wave field representation

We consider a lossless inhomogeneous acoustic medium, which is bounded by a transparent horizontal surface $\partial\mathbb{D}_R$ (the half-space above this surface is homogeneous, with propagation velocity c_0 and mass density ρ_0). The acoustic pressure $p(\mathbf{x}, t)$ in this medium obeys the wave equation $\mathcal{L}p = -\partial_t q$, where \mathcal{L} is the acoustic wave field operator and $q(\mathbf{x}, t)$ is a volume-injection rate source. In this section we discuss an integral representation for p . In the classical approach, wave field representations make use of Green's functions. Here we use focusing functions for the representation. We introduce a focusing function $F(\mathbf{x}, \mathbf{x}_R, t)$ which obeys the source-free wave equation $\mathcal{L}F = 0$ and which focuses at \mathbf{x}_R at $\partial\mathbb{D}_R$, see Figure 1.

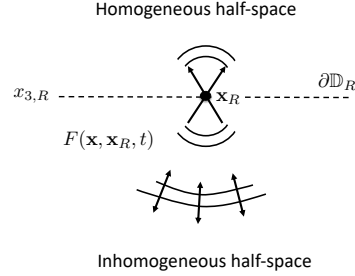


Figure 1: The focusing function $F(\mathbf{x}, \mathbf{x}_R, t)$.

We define \mathbf{x}_R as $\mathbf{x}_R = (\mathbf{x}_{H,R}, x_{3,R})$, where $\mathbf{x}_{H,R}$ is the horizontal position of the focal point and $x_{3,R}$ is the depth of $\partial\mathbb{D}_R$. We define the focusing condition as

$$F(\mathbf{x}, \mathbf{x}_R, t)|_{x_3=x_{3,R}} = \delta(\mathbf{x}_H - \mathbf{x}_{H,R})\delta(t). \quad (1)$$

The wave equation $\mathcal{L}F = 0$, the focusing property of equation 1, and the condition that $F(\mathbf{x}, \mathbf{x}_R, t)$ is upgoing at $\partial\mathbb{D}_R$, together determine the focusing function. Note that inside the inhomogeneous half-space, the focusing function is a full (not decomposed) wave field, which is indicated by the up/down arrows in Figure 1. Only at and above $\partial\mathbb{D}_R$ this function is upgoing, indicated by the upward pointing arrows in Figure 1.

We transform the wave field and focusing function to the frequency domain, giving $p(\mathbf{x}, \omega)$ and $F(\mathbf{x}, \mathbf{x}_R, \omega)$, respectively (ω is the angular frequency). For convenience we use the same symbols p , F and \mathcal{L} in both domains. Hence, the wave equations for p and F in the frequency domain are $\mathcal{L}p = i\omega q$ and $\mathcal{L}F = 0$, respectively (i is the imaginary unit), and the focusing property of equation 1 transforms to

$$F(\mathbf{x}, \mathbf{x}_R, \omega)|_{x_3=x_{3,R}} = \delta(\mathbf{x}_H - \mathbf{x}_{H,R}). \quad (2)$$

We express p in terms of F and F^* (where the asterisk denotes complex conjugation) as follows

$$p(\mathbf{x}, \omega) = \int_{\partial\mathbb{D}_R} F(\mathbf{x}, \mathbf{x}_R, \omega)p^-(\mathbf{x}_R, \omega)d\mathbf{x}_R + \int_{\partial\mathbb{D}_R} F^*(\mathbf{x}, \mathbf{x}_R, \omega)p^+(\mathbf{x}_R, \omega)d\mathbf{x}_R. \quad (3)$$

The superscripts $+$ and $-$ denote downgoing and upgoing waves, respectively, at the boundary $\partial\mathbb{D}_R$.

The representation of equation 3 can be derived by solving two boundary conditions at $\partial\mathbb{D}_R$ (Wapenaar et al., 2021), but here we explain it with intuitive arguments, assuming for the moment that the medium is source-free, hence $\mathcal{L}p = 0$. For \mathbf{x} in the upper half-space, the function $F(\mathbf{x}, \mathbf{x}_R, \omega)$ in the first integral is an upgoing field, which, for \mathbf{x} above $\partial\mathbb{D}_R$, apparently emerges from \mathbf{x}_R at $\partial\mathbb{D}_R$, see Figure 1. Hence, the first integral represents the response to a distribution of Huygens sources

Do we need up/down decomposition?

along $\partial\mathbb{D}_R$, with strength $p^-(\mathbf{x}_R, \omega)$. This gives the forward propagated upgoing field $p^-(\mathbf{x}, \omega)$ in the upper half-space. Similarly, still considering \mathbf{x} in the upper half-space, the function $F^*(\mathbf{x}, \mathbf{x}_R, \omega)$ in the second integral is a downgoing field (ignoring evanescent waves), which, for \mathbf{x} above $\partial\mathbb{D}_R$, converges to \mathbf{x}_R at $\partial\mathbb{D}_R$. Hence, the second integral represents the acausal response to a distribution of Huygens sinks along $\partial\mathbb{D}_R$, with strength $p^+(\mathbf{x}_R, \omega)$. This gives the backward propagated downgoing field $p^+(\mathbf{x}, \omega)$ in the upper half-space. Hence, the sum of the two integrals gives $p^-(\mathbf{x}, \omega) + p^+(\mathbf{x}, \omega) = p(\mathbf{x}, \omega)$ for \mathbf{x} in the upper half-space. However, since equation (3) holds in an entire half-space and since p , F and F^* are solutions of the same wave equation for all \mathbf{x} (i.e., $\mathcal{L}p = \mathcal{L}F = \mathcal{L}F^* = 0$ for all \mathbf{x}), we may conclude that equation (3) holds throughout space. Of course for \mathbf{x} in the lower half-space, the two integrals cannot be separately associated with $p^-(\mathbf{x}, \omega)$ and $p^+(\mathbf{x}, \omega)$; only the sum of the two integrals gives $p(\mathbf{x}, \omega)$. Next, let the source q for the field p be non-zero in the upper half-space $x_3 < x_{3,R}$. Then equation 3 breaks down in the upper half-space, but it still holds in the lower half-space $x_3 \geq x_{3,R}$, where p , F and F^* obey the same source-free wave equation.

Note that we assumed that evanescent waves can be neglected at and above $\partial\mathbb{D}_R$ (by assuming F^* is a downgoing field). However, evanescent waves inside the medium (for example in high-velocity layers) can still be taken into account, as will be illustrated later with a numerical example.

Green's function representation

Equation 3 holds for $x_3 \geq x_{3,R}$ for any wave field $p(\mathbf{x}, \omega)$ obeying $\mathcal{L}p = i\omega q$, as long as q is zero in the lower half-space. Hence, it also holds for the Green's function $G(\mathbf{x}, \mathbf{x}_S, \omega)$, with $\mathcal{L}G = i\omega\delta(\mathbf{x} - \mathbf{x}_S)$, as long as \mathbf{x}_S lies above $\partial\mathbb{D}_R$. Let us choose $\mathbf{x}_S = (\mathbf{x}_{H,S}, x_{3,S})$ just above $\partial\mathbb{D}_R$, hence, $x_{3,S} = x_{3,R} - \epsilon$. We turn the monopole response $G(\mathbf{x}, \mathbf{x}_S, \omega)$ into a dipole source response $\Gamma(\mathbf{x}, \mathbf{x}_S, \omega)$ via

$$\Gamma(\mathbf{x}, \mathbf{x}_S, \omega) = -\frac{2}{i\omega\rho_0} \partial_{3,S} G(\mathbf{x}, \mathbf{x}_S, \omega), \quad (4)$$

where $\partial_{3,S}$ denotes differentiation with respect to the source coordinate $x_{3,S}$. The reason for changing the source type is that the downgoing part of the response to a dipole just below the source position is a simple spatial delta function, hence

$$\Gamma^+(\mathbf{x}, \mathbf{x}_S, \omega)|_{x_3=x_{3,R}} = \delta(\mathbf{x}_H - \mathbf{x}_{H,S}). \quad (5)$$

We define the upgoing part at $\partial\mathbb{D}_R$ of the dipole Green's function as

$$\Gamma^-(\mathbf{x}_R, \mathbf{x}_S, \omega) = R(\mathbf{x}_R, \mathbf{x}_S, \omega), \quad (6)$$

for \mathbf{x}_R at $\partial\mathbb{D}_R$, where $R(\mathbf{x}_R, \mathbf{x}_S, \omega)$ is the reflection response of the inhomogeneous medium below $\partial\mathbb{D}_R$. Replacing p , p^- and p^+ in equation 3 by Γ , Γ^- and Γ^+ , we obtain (using equations 5 and 6)

$$\begin{aligned} \Gamma(\mathbf{x}, \mathbf{x}_S, \omega) &= \int_{\partial\mathbb{D}_R} F(\mathbf{x}, \mathbf{x}_R, \omega) R(\mathbf{x}_R, \mathbf{x}_S, \omega) d\mathbf{x}_R \\ &+ F^*(\mathbf{x}, \mathbf{x}_S, \omega), \quad \text{for } x_3 \geq x_{3,R}. \end{aligned} \quad (7)$$

The Green's function $\Gamma(\mathbf{x}, \mathbf{x}_S, \omega)$ on the left-hand side is a dipole source response. Equation 7 can be modified into a representation for a monopole Green's function (Wapenaar et al.,

2021), which yields

$$\begin{aligned} G(\mathbf{x}, \mathbf{x}_S, \omega) &= \int_{\partial\mathbb{D}_R} f(\mathbf{x}, \mathbf{x}_R, \omega) R(\mathbf{x}_S, \mathbf{x}_R, \omega) d\mathbf{x}_R \\ &+ f^*(\mathbf{x}, \mathbf{x}_S, \omega), \quad \text{for } x_3 \geq x_{3,R}, \end{aligned} \quad (8)$$

where $f(\mathbf{x}, \mathbf{x}_R, \omega)$ is related to $F(\mathbf{x}, \mathbf{x}_R, \omega)$ via

$$F(\mathbf{x}, \mathbf{x}_R, \omega) = \frac{2}{i\omega\rho_0} \partial_{3,R} f(\mathbf{x}, \mathbf{x}_R, \omega), \quad (9)$$

with $f(\mathbf{x}, \mathbf{x}_R, \omega)$ obeying the focusing property

$$\partial_{3,R} f(\mathbf{x}, \mathbf{x}_R, \omega)|_{x_3=x_{3,R}} = \frac{i\omega\rho_0}{2} \delta(\mathbf{x}_H - \mathbf{x}_{H,R}). \quad (10)$$

The representation of equation 8 is similar to our earlier Green's function representation for the Marchenko method, with focusing function f_2 instead of f (Slob et al., 2014; Wapenaar et al., 2014), but it has been derived here without applying up/down decomposition inside the medium. The classical focusing function f_2 is defined in a truncated medium and is related to decomposed focusing functions f_1^+ and f_1^- via

$$f_2(\mathbf{x}_A, \mathbf{x}_R, \omega) = f_1^+(\mathbf{x}_R, \mathbf{x}_A, \omega) - \{f_1^-(\mathbf{x}_R, \mathbf{x}_A, \omega)\}^*. \quad (11)$$

It is important to note that, in general, our new focusing function $f(\mathbf{x}, \mathbf{x}_R, \omega)$ does not obey such a relation, as we demonstrate later. The only conditions for f are the wave equation $\mathcal{L}f = 0$, the focusing property of equation 10 and the requirement that f is upgoing at $\partial\mathbb{D}_R$.

Homogeneous Green's function representation

Replacing the coordinate vectors in equation (8) according to $\mathbf{x}_S \rightarrow \mathbf{x}_R$, $\mathbf{x}_R \rightarrow \mathbf{x}_S$, $\mathbf{x} \rightarrow \mathbf{x}_A$ (and interchanging the source and receiver on the left-hand side) yields

$$\begin{aligned} G(\mathbf{x}_R, \mathbf{x}_A, \omega) &= \int_{\partial\mathbb{D}_R} R(\mathbf{x}_R, \mathbf{x}_S, \omega) f(\mathbf{x}_A, \mathbf{x}_S, \omega) d\mathbf{x}_S \\ &+ f^*(\mathbf{x}_A, \mathbf{x}_R, \omega), \quad \text{for } x_{3,A} \geq x_{3,R}. \end{aligned} \quad (12)$$

In this form, the representation describes source-redatuming from all \mathbf{x}_S at the surface to virtual-source position \mathbf{x}_A in the subsurface. Next, we want to redatum the receivers from all \mathbf{x}_R at the surface to virtual-receiver position \mathbf{x} in the subsurface. We cannot substitute $G(\mathbf{x}, \mathbf{x}_A, \omega)$ for $p(\mathbf{x})$ in equation 3, since $G(\mathbf{x}, \mathbf{x}_A, \omega)$ has its source below $\partial\mathbb{D}_R$. However, the homogeneous Green's function $G_h(\mathbf{x}, \mathbf{x}_A, \omega) = G(\mathbf{x}, \mathbf{x}_A, \omega) + G^*(\mathbf{x}, \mathbf{x}_A, \omega)$ (Porter, 1970; Oristaglio, 1989) obeys $\mathcal{L}G_h = 0$ and hence can be substituted for $p(\mathbf{x})$ in equation 3. At $\partial\mathbb{D}_R$ the Green's function $G(\mathbf{x}, \mathbf{x}_A, \omega)$ is purely upgoing, since \mathbf{x}_A lies below $\partial\mathbb{D}_R$ and the half-space above $\partial\mathbb{D}_R$ is homogeneous, hence $p^-(\mathbf{x}_R, \omega) = G(\mathbf{x}_R, \mathbf{x}_A, \omega)$ and $p^+(\mathbf{x}_R, \omega) = G^*(\mathbf{x}_R, \mathbf{x}_A, \omega)$ for \mathbf{x}_R at $\partial\mathbb{D}_R$ (again ignoring evanescent waves at $\partial\mathbb{D}_R$). With these substitutions, equation 3 yields

$$\begin{aligned} G_h(\mathbf{x}, \mathbf{x}_A, \omega) &= \int_{\partial\mathbb{D}_R} F(\mathbf{x}, \mathbf{x}_R, \omega) G(\mathbf{x}_R, \mathbf{x}_A, \omega) d\mathbf{x}_R \\ &+ \int_{\partial\mathbb{D}_R} F^*(\mathbf{x}, \mathbf{x}_R, \omega) G^*(\mathbf{x}_R, \mathbf{x}_A, \omega) d\mathbf{x}_R, \end{aligned} \quad (13)$$

or

$$G_h(\mathbf{x}, \mathbf{x}_A, \omega) = 2\Re \int_{\partial\mathbb{D}_R} F(\mathbf{x}, \mathbf{x}_R, \omega) G(\mathbf{x}_R, \mathbf{x}_A, \omega) d\mathbf{x}_R, \quad (14)$$

Do we need up/down decomposition?

where \Re denotes the real part. Similar homogeneous Green's function representations have previously been derived by Wapenaar et al. (2016), Van der Neut et al. (2017) and Singh and Snieder (2017), but here we avoided up/down decomposition in the subsurface. The combination of equations 12 and 14 describes a two-step procedure for redatuming the sources and receivers from \mathbf{x}_S and \mathbf{x}_R at the surface to \mathbf{x}_A and \mathbf{x} , respectively, in the subsurface. This two-step process generalises classical primary redatuming (Berkhout, 1982; Berryhill, 1984) to full wavefield redatuming, accounting for primaries, multiples and evanescent waves. It can be further generalised for elastodynamic waves (Wapenaar et al., 2021).

Numerical examples

Although evanescent waves are not the main motivation for deriving the new representations, we illustrate the representations with numerical examples for a horizontally layered medium with high-velocity layers with tunneling evanescent waves. For a horizontally layered medium we consider oblique plane waves in the slowness intercept-time (s_1, τ) domain. In this domain, equation 8 transforms to

$$G(s_1, x_3, x_{3,R}, \tau) = \int_{-\infty}^{\tau} f(s_1, x_3, x_{3,R}, \tau') R(s_1, x_{3,R}, \tau - \tau') d\tau' + f(s_1, x_3, x_{3,R}, -\tau), \quad \text{for } x_3 \geq x_{3,R}, \quad (15)$$

with $f(s_1, x_3, x_{3,R}, \tau)$ obeying the focusing property

$$f(s_1, x_3, x_{3,R}, \tau)|_{x_3=x_{3,R}} = \frac{\rho_0 c_0}{2 \cos \alpha_0} \delta(\tau), \quad (16)$$

where $\alpha_0 = \arcsin(s_1 c_0)$. We consider an oblique plane wave, with $s_1 = 1/2800$ s/m, incident from $\partial\mathbb{D}_R$ to the horizontally layered medium of Figure 2a. This wave becomes evanescent in the two high-velocity layers, with $c_2 = c_4 = 3000$ m/s. The reflection response $R(s_1, x_{3,R}, \tau)$, convolved with a Ricker wavelet with a central frequency of 50 Hz, is shown in Figure 2b. The numerically modelled classical focusing function $f_2(s_1, x_3, x_{3,R}, \tau)$ (equation 11) is shown in Figure 2c. It exhibits the expected behavior in the low-velocity layers with $c_1 = c_3 = c_5 = 2000$ m/s, but the tunneling in the high-velocity layers is wrong, see the panel on the right, which shows the normalized power-flux as a function of depth. Figure 2d shows the numerically modelled focusing function $f(s_1, x_3, x_{3,R}, \tau)$ (which does not make use of equation 11), with correct tunneling behavior in the high-velocity layers.

Next, the Green's function $G(s_1, x_3, x_{3,R}, \tau)$ is derived from the reflection response of Figure 2b and the focusing function, using equation 15. First we use the classical focusing function f_2 of Figure 2c. The result is shown in Figure 3a. This Green's function shows the expected behavior in the low-velocity layers, but inside the high-velocity layers the retrieved Green's function is wrong. This is emphasised in Figure 3b, which shows the retrieved Green's function at $x_3 = x_{3,A} = 210$ m, halfway the first high-velocity layer (green), compared with the exact Green's function (red). We repeat the same process, but this time with the correct focusing function f of Figure 2d. The results are shown in Figures 3c and d. Note that this time the Green's function is perfectly retrieved, in the low- and high-velocity layers. This confirms that the representation of equation 15 correctly accounts for evanescent waves.

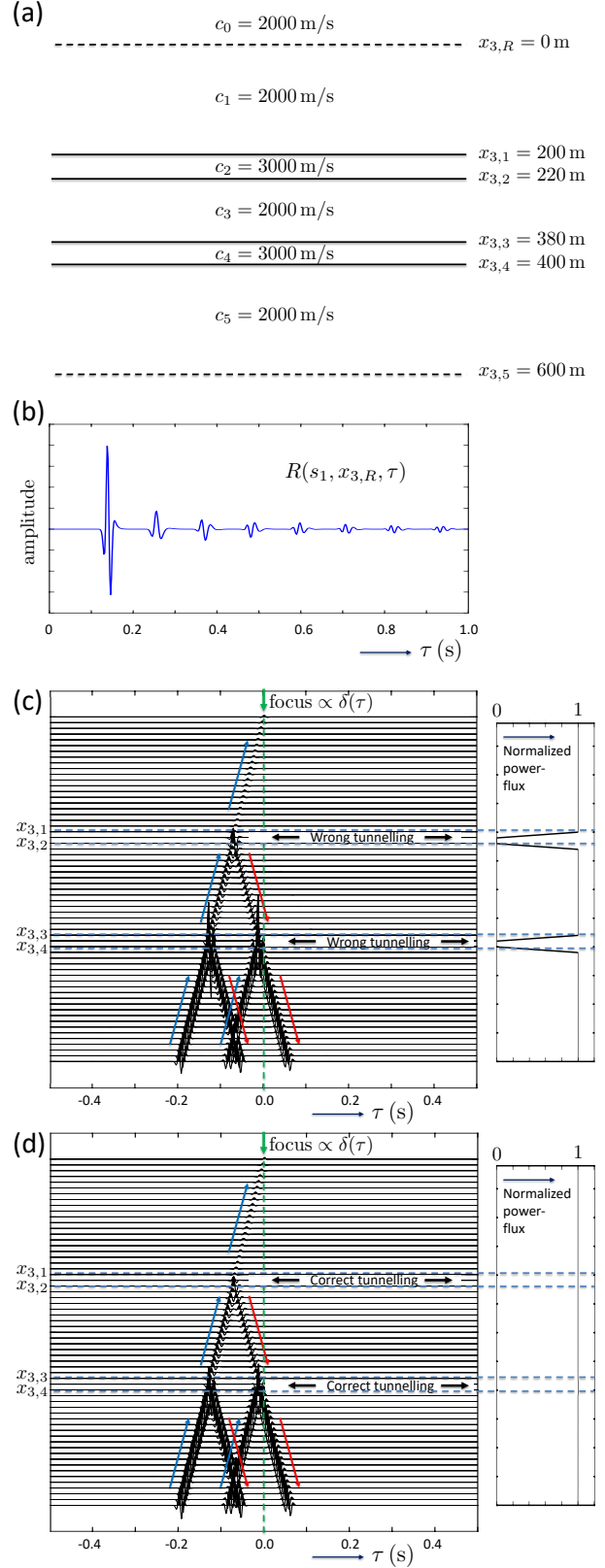


Figure 2: (a) Horizontally layered medium. (b) Reflection response $R(s_1, x_{3,R}, \tau)$ at the surface. (c) Numerically modelled classical focusing function $f_2(s_1, x_3, x_{3,R}, \tau)$. (d) Numerically modelled new focusing function $f(s_1, x_3, x_{3,R}, \tau)$.

Do we need up/down decomposition?

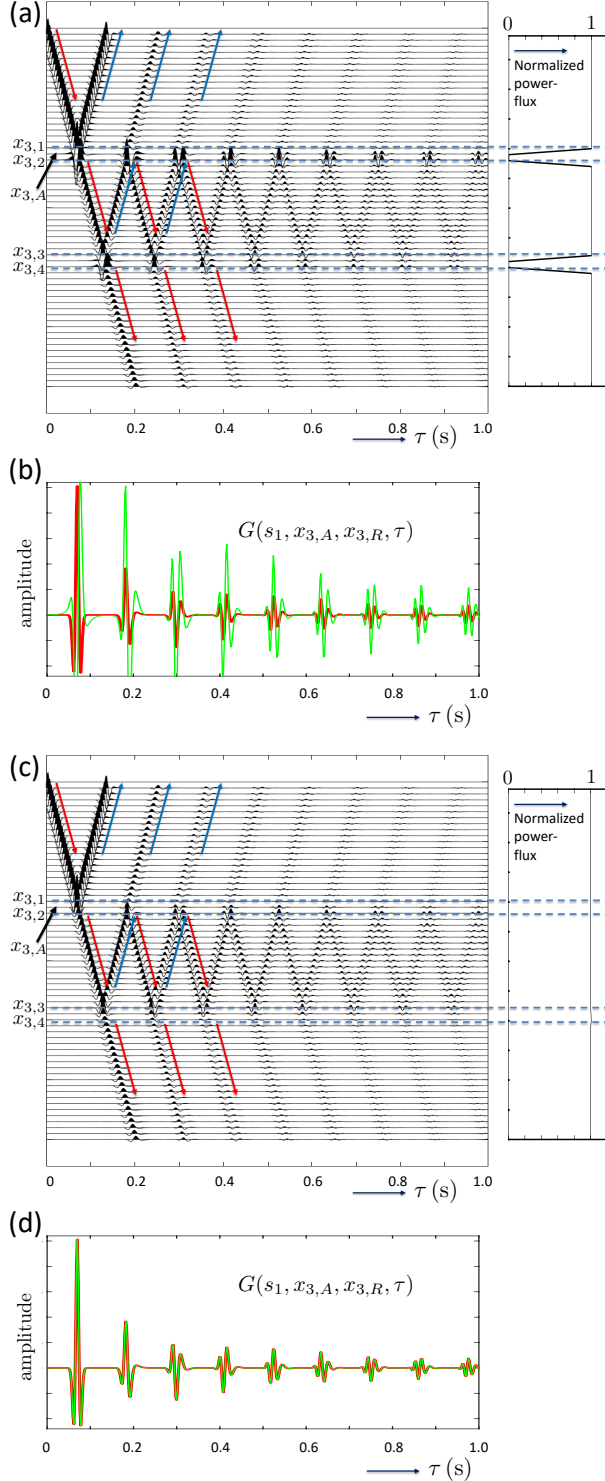


Figure 3: (a) Green's function $G(s_1, x_3, x_{3,R}, \tau)$ obtained from Figures 2(b) and 2(c) via the representation of equation (15). (b) $G(s_1, x_{3,A}, x_{3,R}, \tau)$, taken from figure (a) for $x_{3,A} = 210$ m (green), compared with directly modelled Green's function (red). (c) Green's function $G(s_1, x_3, x_{3,R}, \tau)$ obtained from Figures 2(b) and 2(d) via the representation of equation (15). (d) $G(s_1, x_{3,A}, x_{3,R}, \tau)$, taken from figure (c) for $x_{3,A} = 210$ m, compared with directly modelled Green's function.

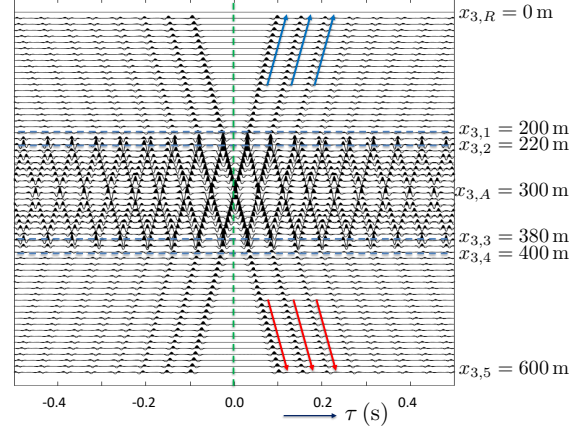


Figure 4: Homogeneous Green's function $G_h(s_1, x_3, x_{3,A}, \tau)$ for $x_{3,A} = 300$ m, obtained from representation 17.

Finally, we transform the representation of equation (13) to the slowness intercept-time domain, hence

$$G_h(s_1, x_3, x_{3,A}, \tau) = \int_{-\infty}^{\tau} F(s_1, x_3, x_{3,R}, \tau') G(s_1, x_{3,R}, x_{3,A}, \tau - \tau') d\tau' + \int_{\tau}^{\infty} F(s_1, x_3, x_{3,R}, -\tau') G(s_1, x_{3,R}, x_{3,A}, \tau' - \tau) d\tau', \quad (17)$$

with

$$F(s_1, x_3, x_{3,R}, \tau) = \frac{2 \cos \alpha_0}{\rho_0 c_0} f(s_1, x_3, x_{3,R}, \tau). \quad (18)$$

Using the focusing function of Figure 2d and the Green's function of Figure 3c, this time for fixed $x_{3,A} = 300$ m, equation 17 gives the homogeneous Green's function shown in Figure 4. The causal part is the response to a virtual source at $x_{3,A} = 300$ m, observed by virtual receivers at variable x_3 . Note the reverberations in the wave guide between the high-velocity layers, and the leaking of energy via tunneling through the high-velocity layers. This example shows that also the homogeneous Green's function representation of equation 17 accounts for propagating and evanescent waves.

Conclusions

We have shown that the Green's function representations for the Marchenko method can be derived without assuming the fields inside the medium can be decomposed into downgoing and upgoing waves and without ignoring evanescent waves inside the medium. These representations have potential applications in the development of new Marchenko methods that can take refracted and evanescent waves into account. However, this development will also need careful consideration of the temporal overlap of Green's functions and focusing functions.

Acknowledgements

We acknowledge funding from the European Research Council (ERC) under the European Union's Horizon 2020 research and innovation programme (grant agreement No: 742703).

Do we need up/down decomposition?

REFERENCES

- Berkhout, A. J., 1982, Seismic Migration. Imaging of acoustic energy by wave field extrapolation. A. Theoretical aspects: Elsevier.
- Berryhill, J. R., 1984, Wave-equation datuming before stack: *Geophysics*, **49**, 2064–2066.
- Brackenhoff, J., J. Thorbecke, and K. Wapenaar, 2019, Monitoring of induced distributed double-couple sources using Marchenko-based virtual receivers: *Solid Earth*, **10**, 1301–1319.
- Diekman, L., and I. Vasconcelos, 2021, Focusing and Green's function retrieval in three-dimensional inverse scattering revisited: A single-sided Marchenko integral for the full wave field: *Physical Review Research*, **3**, 013206.
- Elison, P., M. S. Dukalski, K. de Vos, D. J. van Manen, and J. O. A. Robertsson, 2020, Data-driven control over short-period internal multiples in media with a horizontally layered overburden: *Geophysical Journal International*, **221**, 769–787.
- Jia, X., A. Guitton, and R. Snieder, 2018, A practical implementation of subsalt Marchenko imaging with a Gulf of Mexico data set: *Geophysics*, **83**, S409–S419.
- Kiraz, M. S. R., R. Snieder, and K. Wapenaar, 2020, Marchenko focusing without up/down decomposition: 90th Annual International Meeting, SEG, Expanded Abstracts, 3593–3597.
- Lomas, A., and A. Curtis, 2019, An introduction to Marchenko methods for imaging: *Geophysics*, **84**, F35–F45.
- Mildner, C., F. Brogini, K. de Vos, and J. O. A. Robertsson, 2019, Accurate source wavelet estimation using Marchenko focusing functions: *Geophysics*, **84**, Q73–Q88.
- Oristaglio, M. L., 1989, An inverse scattering formula that uses all the data: *Inverse Problems*, **5**, 1097–1105.
- Pereira, R., M. Ramzy, P. Griscenco, B. Huard, H. Huang, L. Cypriano, and A. Khalil, 2019, Internal multiple attenuation for OBN data with overburden/target separation: 89th Annual International Meeting, SEG, Expanded Abstracts, 4520–4524.
- Porter, R. P., 1970, Diffraction-limited, scalar image formation with holograms of arbitrary shape: *Journal of the Optical Society of America*, **60**, 1051–1059.
- Ravasi, M., and I. Vasconcelos, 2020, On the implementation of large-scale integral operators with modern HPC solutions – Application to 3D Marchenko imaging by least-squares inversion: arXiv:2011.11120.
- Ravasi, M., I. Vasconcelos, A. Kritski, A. Curtis, C. A. da Costa Filho, and G. A. Meles, 2016, Target-oriented Marchenko imaging of a North Sea field: *Geophysical Journal International*, **205**, 99–104.
- Reinicke, C., M. Dukalski, and K. Wapenaar, 2020, Comparison of monotonicity challenges encountered by the inverse scattering series and the Marchenko demultiple method for elastic waves: *Geophysics*, **85**, Q11–Q26.
- Singh, S., and R. Snieder, 2017, Source-receiver Marchenko redatuming: Obtaining virtual receivers and virtual sources in the subsurface: *Geophysics*, **82**, Q13–Q21.
- Slob, E., K. Wapenaar, F. Brogini, and R. Snieder, 2014, Seismic reflector imaging using internal multiples with Marchenko-type equations: *Geophysics*, **79**, S63–S76.
- Staring, M., R. Pereira, H. Douma, J. van der Neut, and K. Wapenaar, 2018, Source-receiver Marchenko redatuming on field data using an adaptive double-focusing method: *Geophysics*, **83**, S579–S590.
- Staring, M., and K. Wapenaar, 2020, Three-dimensional Marchenko internal multiple attenuation on narrow azimuth streamer data of the Santos Basin, Brazil: *Geophysical Prospecting*, **68**, 1864–1877.
- Van der Neut, J., J. L. Johnson, K. van Wijk, S. Singh, E. Slob, and K. Wapenaar, 2017, A Marchenko equation for acoustic inverse source problems: *Journal of the Acoustical Society of America*, **141**, 4332–4346.
- Wapenaar, K., R. Snieder, S. de Ridder, and E. Slob, 2021, Green's function representations for Marchenko imaging without up/down decomposition: arXiv:2103.07734.
- Wapenaar, K., J. Thorbecke, and J. van der Neut, 2016, A single-sided homogeneous Green's function representation for holographic imaging, inverse scattering, time-reversal acoustics and interferometric Green's function retrieval: *Geophysical Journal International*, **205**, 531–535.
- Wapenaar, K., J. Thorbecke, J. van der Neut, F. Brogini, E. Slob, and R. Snieder, 2014, Marchenko imaging: *Geophysics*, **79**, WA39–WA57.
- Zhang, L., and E. Slob, 2020, A fast algorithm for multiple elimination and transmission compensation in primary reflections: *Geophysical Journal International*, **221**, 371–377.